

Mechanical Properties of Laser Beam Welded Dissimilar High Strength Steels: 300M and DP 780

A. T. Harada^{a*}, E. G. S. Zanni^a, L. S. Aota^b, K. D. Zilnyk^a, M. S. F. Lima^{a,c}, A. J. Abdalla^{a,c}

^aInstituto Tecnológico de Aeronáutica (ITA), São José dos Campos, SP, Brasil.

^bMax-Planck - Institut für Eisenforschung, 40237 Düsseldorf, Alemanha.

^cInstituto de Estudos Avançados (IEAv), São José dos Campos, SP, Brasil.

Received: January 16, 2023; Revised: May 29, 2023; Accepted: June 07, 2023

Aerospace and automotive industries utilize advanced high strength steels due to their exceptional mechanical strength and ductility. Laser beam welding has shown potential in reducing the melted zone, heat affected zone, and process time for these steels. This study focused on dissimilar welding between DP 780 and 300M steel sheets, commonly used in the automotive and aerospace industries, respectively. The aim was to expand the range of possibilities and innovations by enabling the use of these steels in both applications. The study investigated the optimal process parameters, microstructure, and mechanical properties for the laser welding process. It also examined the influence of intercritical quenching and tempering on the microstructure and mechanical properties of the laser welded steels. The materials underwent dilution and different phase transformations due to the welding process and heat treatments, as revealed by microstructural characterization. The weld showed a notable increase in hardness, however without compromising toughness. The fractures during tensile testing occurred in the DP 780 steel, far from the MZ and HAZ. Heat treatments increased ultimate tensile strength, but lowered ductility. Welding affected the fatigue life, especially in the intercritically quenched joint, which showed a quasi-cleavage crack growth mechanism and a decrease in fracture toughness.

Keywords: laser beam welding, advanced high strength steels, dissimilar welding, heat treatments, mechanical properties.

1. Introduction

Ultra-high strength steels (UHSS) are used where a high strength-to-weight ratio is required, along with high toughness and ductility. The 300M steel has an excellent combination of these properties and due to an increase in silicon and molybdenum contents and the addition of vanadium in the composition, this steel can maintain high levels of ductility and tenacity even at tensile strength limits up to 2070 MPa. It is used in several applications in the aeronautical and aerospace industries such as landing gear structures, rocket engine envelopes and joints of satellite launch vehicle parts¹⁻⁴.

The 300M steel is weldable by most processes, both conventional and laser. However, a hardening of the melted zone is observed, which increases the susceptibility to cracks, due to possible local reductions in the material properties⁵⁻⁷.

Advanced high strength steels (AHSS), initially developed for the automotive industry, have the potential to partially replace more expensive steels, such as UHSS, in certain applications in the aerospace sector. These steels have a very controlled chemical composition and go through specific thermal and thermomechanical treatments, resulting in complex microstructures composed of different phases and in an excellent resistance/ductility ratio^{4,8-13}.

Due to the complex microstructure of AHSS, it is necessary to understand the welding process of these steels and consider

possible implications for their microstructure and properties, especially in the heat affected zone (HAZ)^{4,9,10,14}. Among the various types of AHSS, dual phase (DP) steels are considered excellent options for aerospace applications^{12,14-17}, being able to reach different degrees of resistance, which reach up to 1000 MPa, maintaining good ductility in addition to excellent energy absorption in mechanical impact conditions.

The combination of ultra-high strength aeronautical steels and high strength steels with dual phase structures can expand the range of application possibilities and innovations¹¹. In this work, we report the laser welding of a DP 780 steel, a third generation AHSS steel, to a 300M UHSS steel. The objective is to assess the possibility of producing dissimilar welded joints of these steels with adequate mechanical properties^{5,7,14,18}. Two different heat treatment sequences were tested. Optical microscopy and scanning electron microscopy coupled with electron backscattered diffraction were used to characterize the resulting microstructures. Vickers microhardness, tensile tests and uniaxial fatigue tests were employed to evaluate the mechanical properties of the welded joints.

2. Experimental Procedure

Sheets of 300M and DP 780 steels were used, with an area of approximately 200 cm² (20x20 cm) and thicknesses of 3.2 mm and 2.6 mm, respectively. The chemical composition of these steels is shown in Table 1 as supplied by manufacturer

*e-mail: anaharada@yahoo.com.br

Table 1. Chemical composition of 300M and DP 780 steels.

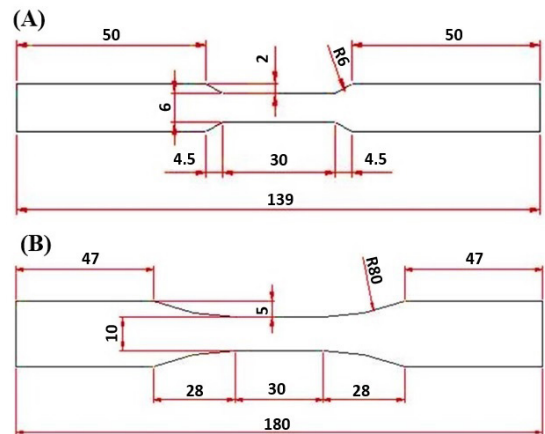
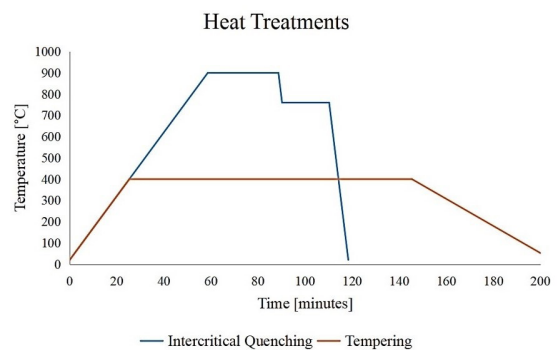
	C	S	P	Si	Cr	Mo	Al	Ni	V	Mn	Nb	Ti
300M	0.390	0.0005	0.009	1.78	0.76	0.40	0.003	1.69	0.08	-	-	-
DP 780	0.086	0.0070	0.027	0.05	0.05	0.23	0.003	-	-	1.739	0.028	0.004

Table 2. Welding parameters.

Laser Power	Welding Speed	Number of Passes	Protection Gas Flow
1800 W	50 mm/s	2	8 L/min (Argon)

Companhia Siderúrgica Nacional – CSN/Volta Redonda, Brazil (DP 780) and by the Institute of Aeronautics and Space – IAE/São José dos Campos, Brazil (300M). A 2 kW fiber laser, IPG, YRL-2000, was used ($\lambda = 1.046$ nm), in continuous mode. The welding parameters used are shown in Table 2. The laser beam was kept in focus (focal length of 160 mm) in relation to the thinner sheet plate (DP 780). Two laser passes were applied, one at the top and one at the bottom of the sheets, so that there was a straight bead on both sides, since the sheets have different thicknesses. Before welding, the edges of the sheets were grinded in order to reduce the risk of porosity in the welded joint and to protect the material from possible contaminants from the cutting process. The microhardness tests were carried out with a Vickers microhardness tester. The test load used was 100 gf (0,98 N), with a loading time of 9 seconds. The measurements were performed covering the base metals, the heat affected zones and the melted zone, with a 50 μ m step between measurements, resulting in an average of 25 indentations in each sample. Specimens were machined by wire EDM (Electric Discharge Machining) for mechanical tests, according to ASTM E8/E8M (Tensile) and E466 (Fatigue) standard, shown in Figure 1A and Figure 1B, respectively. In tensile tests, an EMIC DL 63 100 kN with a test speed of 1 mm/min at room temperature was used. During tensile tests, for accurate monitoring the strain, an electronic strain gauge, EMIC EE09, was fitted in the specimen. The uniaxial fatigue tests were conducted with a load ratio equal to 0.1 and a frequency of 25 Hz with a 250 kN load cell, using an MTS 810.23M. The microstructure analyses of the welded joint were performed with an optical microscope (OM) and scanning electron microscope (SEM). Electron Backscatter Diffraction (EBSD) was performed in as-polished samples using a JEOL-6500F SEM equipped with a TSL TexSEM DigiView EBSD camera. For the microstructural characterization of the samples, a chemical etching with 3% nital was used. The heat treatment profiles, with temperatures and times used in the process, are shown in Figure 2.

An electric resistive furnace was used for the intercritical quenching treatment. The specimens were heated at a rate of 15 °C/min to a level of 900 °C for 30 minutes, after that, the specimen was transferred to another similar furnace, at a temperature of 760 °C for 20 minutes (to obtain the formation of the ferrite phase) and finally, cooling by quenching in oil (to obtain the formation of the martensite phase). For the tempering treatment, the same furnace for the intercritical quenching was used. The specimen was introduced at a temperature of 400 °C for 2 hours and cooled to room temperature in calm air afterwards.

**Figure 1.** Specimen in mm for (A) tensile tests and (B) fatigue tests^{19,20}.**Figure 2.** Heat treatments profile: Intercritical quenching and tempering.

3. Results and Discussion

3.1. Microstructural characterization

The 300M steel microstructure, shown in Figure 3A, indicates the presence of a ferritic phase with pearlite microconstituent, average hardness of 278 HV, and annealed characteristics like equiaxed grains. The DP 780 steel microstructure, shown in Figure 3B, indicates a ferritic and martensitic matrix, where the light region is ferrite and the dark region is martensite. In addition to the average hardness of 226 HV. These observations are similar to previous works⁸.

In the macrographs, shown in Figure 4A and Figure 4B, observed narrow weld beads and a HAZ with a reduced size, characteristics considered positive, since defects and fragility are favorable in these regions. Also, no pores are observed on welds, indicating an appropriate selection of welding parameters.

With higher magnifications, in Figure 5A and Figure 5B, it is possible to observe the dilution between the materials and morphological differences in the MZ of the welds submitted to the tempering treatment: (1) the formation of martensite phase in the region of the 300M steel, associated to the higher

percentage of C and Si on composition, to the rapid cooling of the process and (2) the formation of a higher percentage of ferrite phase close to the region of DP 780 steel.

From the center of the MZ, observed that the grains tend to elongate to the sides, due to heat extraction when solidification occurs. There is a presence of phases as acicular ferrite (with the sample of elongated needles) and retained austenite and polygonal ferrite on the martensitic matrix.

Figure 6, showing the MZ of the weld with the intercritical tempering treatment, is possible observed a predominance of the martensitic phase, indicating the dilution of chemical

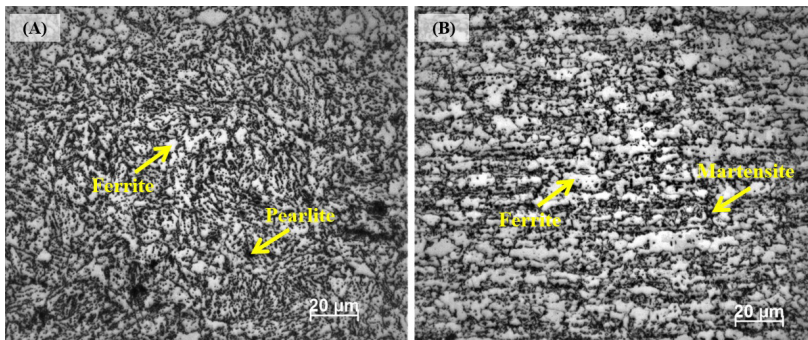


Figure 3. Optical Micrography (OM): Base metal micrography (A) 300M and (B) DP 780.

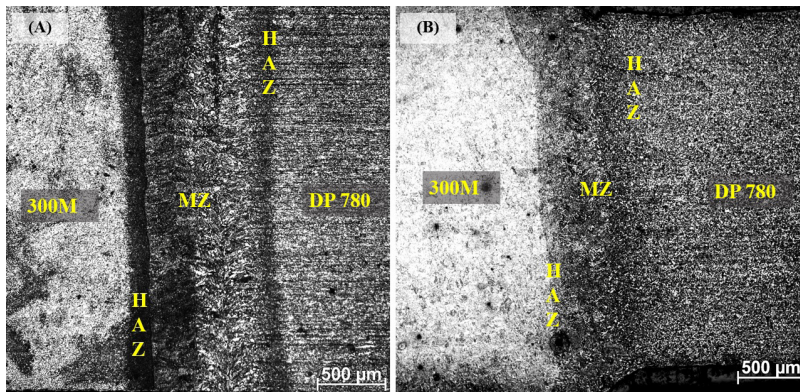


Figure 4. OM: laser welded 300M and DP 780 steels in condition (A) tempering and (B) intercritical quenching.

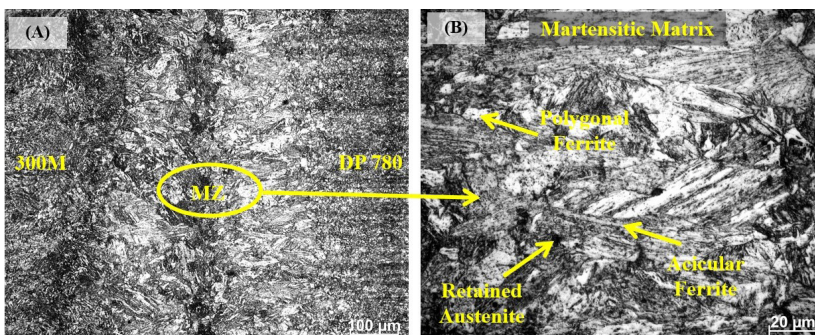


Figure 5. OM: (A) laser welded 300M and DP 780 steels and (B) Melted zone after tempering.

elements present in the composition of the 300M steel to the center of the pool during the melting. In addition to small regions corresponding to ferritic phase.

In the HAZ of welds with tempering and as-welded, a morphological change is observed in the 300M region, shown in Figure 7A, indicating phase transformation: pearlite – austenite – martensite. The formation of martensite, as previously mentioned, is associated with rapid cooling after the welding process and the composition of the 300M steel. In the region not affected by heat, a ferritic-pearlitic microstructure can be seen, typical of this steel.

In the DP 780 steel, shown in Figure 7B, in the region designated by number 1, the grains have a larger size, due to this region reached a high temperature for austenitization and grain growth. In region designated by number 2, it is possible observed occurrence phase transformation too: ferrite – austenite – ferrite. The grains have a reduced size due to a shorter time the region was subjected to a high temperature. And in the region designated by number 3, the microstructure is similar to the base metal.

In the EBSD maps shown in Figure 8A; Figure 8B; Figure 8C and Figure 8D, Figure 9A and Figure 9B; Figure 10; Figure 11A, Figure 11B and Figure 11C and Figure 12A, Figure 12B and Figure 12C more details of microstructural characterization of MZ and HAZ of welds with the 3 conditions

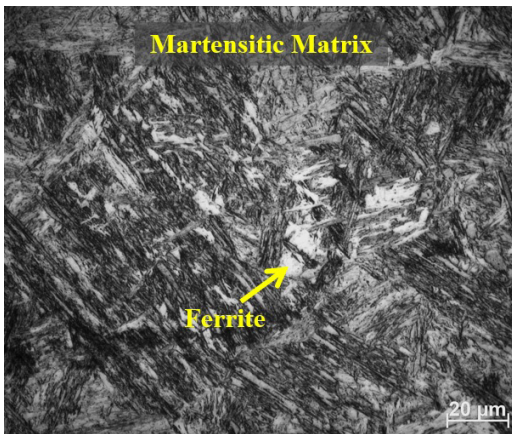


Figure 6. OM: laser welded 300M and DP 780 steels melted zone after intercritical quenching – showing region with martensitic predominance and small regions of ferritic phase.

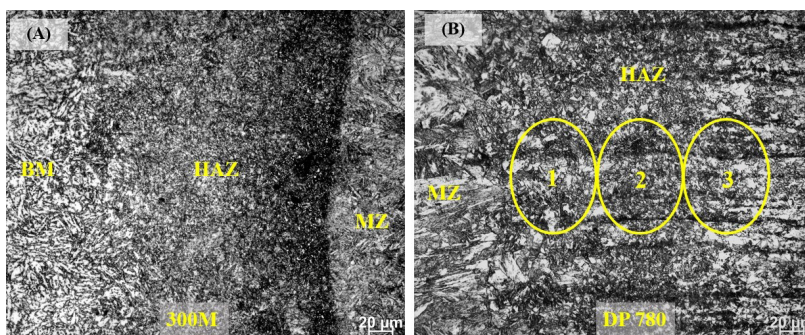


Figure 7. MO: HAZ and MZ after tempering treatment (A) 300M (B) DP 780 steels.

proposed in this study and the microhardness profile obtained through microhardness tests.

The microstructure of 300M steel HAZ and BM regions, for welds with intercritical quenching, are similar without significant variations associated to effects of heat treatment, due to the higher carbon content (0.39%) and of Si (1.78%), which favor the formation of martensitic microstructure. In both regions, formed ferritic phase and/or retained austenite. For DP 780, compared to the as-welded sample and the base metal, although the microstructures are dual phase (ferrite + martensite), is observed a grain growth and a correction of deformations and grain orientations due to the rolling process. In addition to, an increase in the volume fraction of the martensitic phase is observed. Figure 13A and Figure 13B shown the microstructures of 300M and DP 780 steels after intercritical quenching.

3.2. Microhardness tests

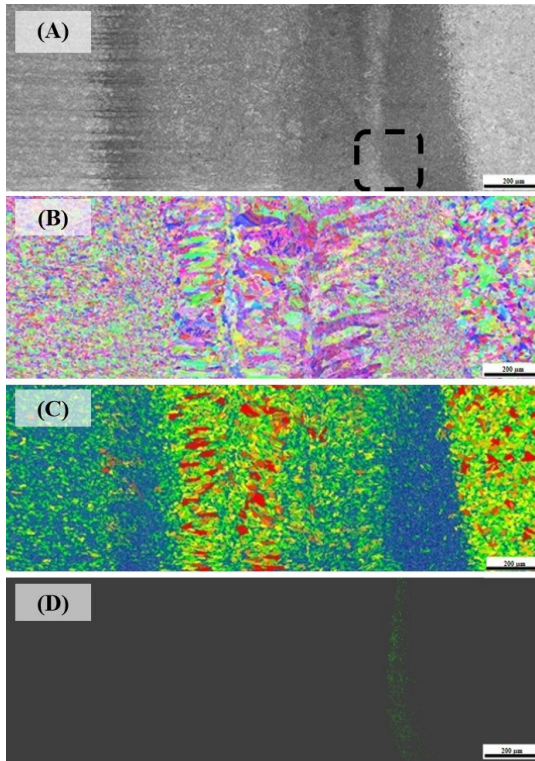
In the microhardness tests, 1 specimen of each condition was analyzed to monitor alterations associated with heat treatments in different regions. Figure 14A shows the microhardness profile of the as-welded specimen, was observed a high hardness in the MZ due to a predominance of martensite, as previously presented. In both HAZ (300M and DP 780), there is an increased hardness compared to the BM, with the highest hardness in the 300M steel region, associated with the elements present in the composition of DP 780 steel.

Figure 14B shows the microhardness profile of the weld with tempering treatment, which was observed similarities to the as-welded specimens in the BM region. Some variations in the HAZ of 300M steel and the MZ, associated with the treatment act as a “stress reliever”, explain a reduction hardness in the BM of 300M steel and in the HAZ and MZ, regions considered to concentrate residual stresses and where the volume of martensite is greater. The decrease in the HAZ of 300M steel, may indicate the production of tempered martensite, and the increase in the BM of DP 780, may indicate an aging process associated with the diffusion of interstitial elements, mainly carbon.

Figure 14C shows the microhardness profile of the weld with intercritical quenching treatment. A gradual increase in hardness is observed, starting at DP 780 steel to 300M steel, indicating a variation in the content of carbon and substitution elements (Cr, Mo, Ni, and V), associated with

Table 3. Mechanical properties in tensile tests of laser welded specimens with heat treatments and as-welded.

Conditions	UTS (MPa)	σ_y (MPa)	Elongation (%)	Rupture
W	776 ± 8	611 ± 27	17 ± 2	BM - DP 780
IQ	969 ± 10	842 ± 53	11 ± 2	BM - DP 780
T	775 ± 6	670 ± 3	16 ± 1	BM - DP 780

**Figure 8.** EBSD mappings of the as-welded sample showing (A) Image quality map; (B) MO inverse pole figure orientation map; (C) grain size map and (D) phase map, showing BCC in dark gray and FCC in green.

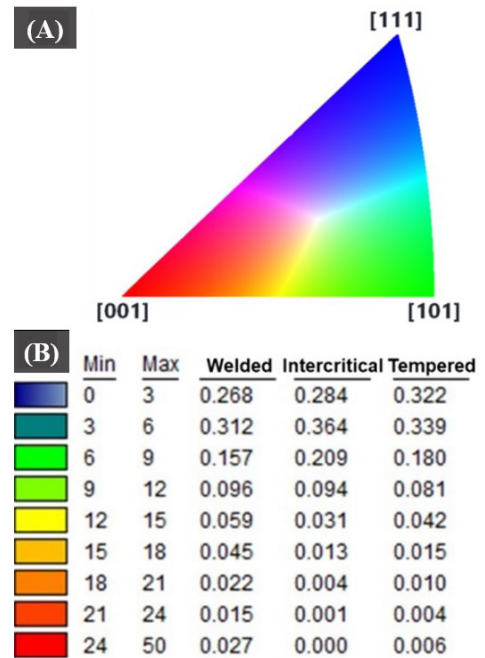
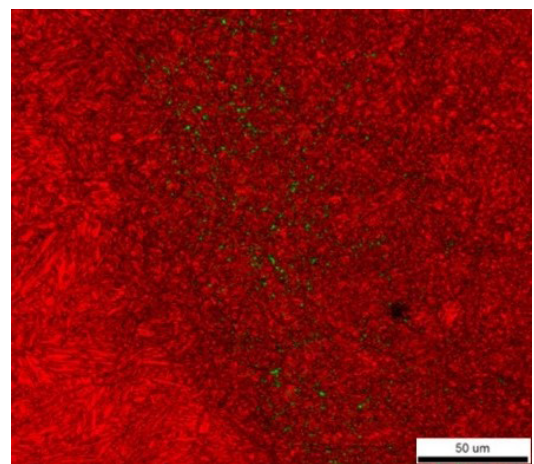
the dilution process between the two steels in MZ, which created a decreasing gradient in these elements. In addition, in the MZ, the hardness was lower compared to as-welded specimens, once the intercritical quenching treatment supported the formation of ferrite.

3.3. Tensile tests

In the tensile tests, 3 specimens of each condition were analyzed. In all specimens of all conditions, the ruptures occurred on the DP 780 steel, which has a lower ultimate strength^{12,14-17}. Figure 15 shows representative engineering stress x strain curves of the 3 studied conditions. Table 3 shows the average results of the main mechanical properties.

In the as-welded specimens, the ultimate strength is compatible with DP 780 steel (about 750 and 800 MPa) and a good ductility (about 17% of elongation), associated with the ferritic phase in the microstructure.

In the specimens with tempering treatment, the ultimate strength and elongation are similar to specimens as-welded but, with a yield strength increase of approximately

**Figure 9.** (A) Inverse Pole Figure Color Coding of Orientation Maps and (B) Color code and area fractions for grain size map. Condition: As-welded.**Figure 10** - Enlarged view of featured HAZ region shown in Figure 8A. IQ+ Phase map showing BCC in red and FCC in green. Condition: As-welded.

40 MPa, may be associated to the aging effects noted in the microhardness tests. Also indicates a better accommodation of the microstructure, reducing the internal stresses, that

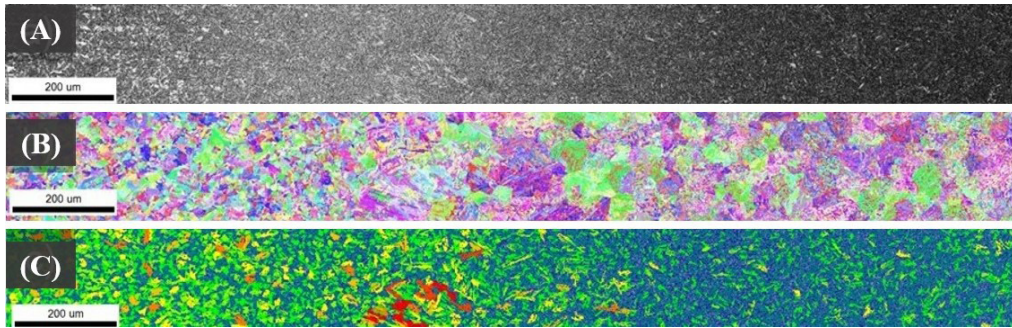


Figure 11. EBSD mappings of the tempering sample showing (A) Image quality map; (B) inverse pole figure orientation map and (C) grain size map.

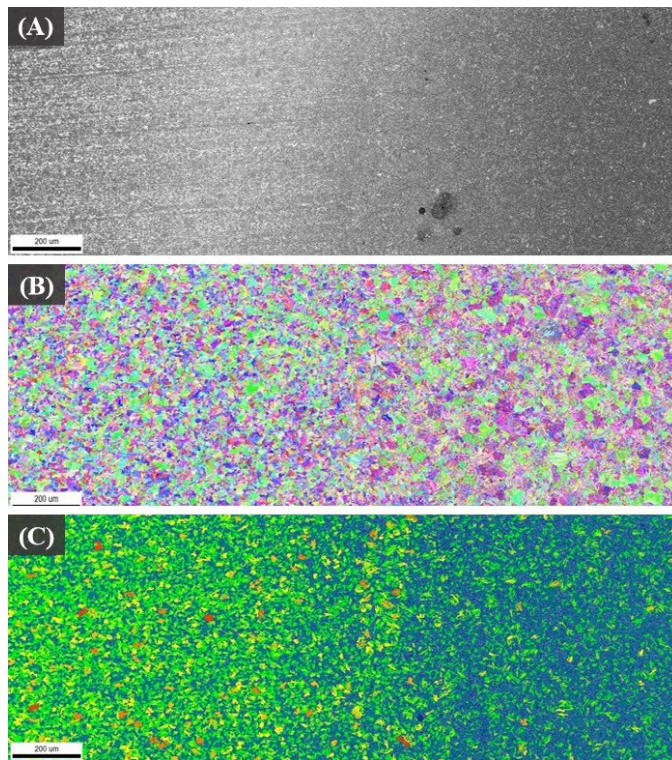


Figure 12. EBSD mappings of the intercritical quenching sample showing: (A) Image quality map; (B) inverse pole figure orientation map; (C) grain size map.

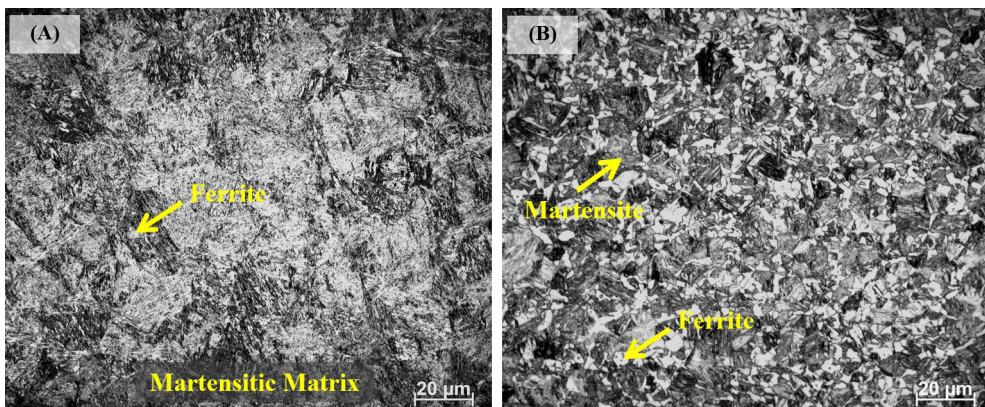


Figure 13. Base metal microscopy after intercritical quenching (A) 300M and (B) DP 780.

may be associated with the initial laminated structure of the DP 780 steel.

In the specimens with intercritical quenching, the ultimate strength and the yield strength are higher than in as-welded

specimens and after tempering, however, there was a reduction in stretching to about 11%, associated with the increase of martensite in the microstructure after heat treatment, but maintain the ductility due to ferrite. The maximum stress levels reached in the tensile tests were not enough to deform the 300M steel.

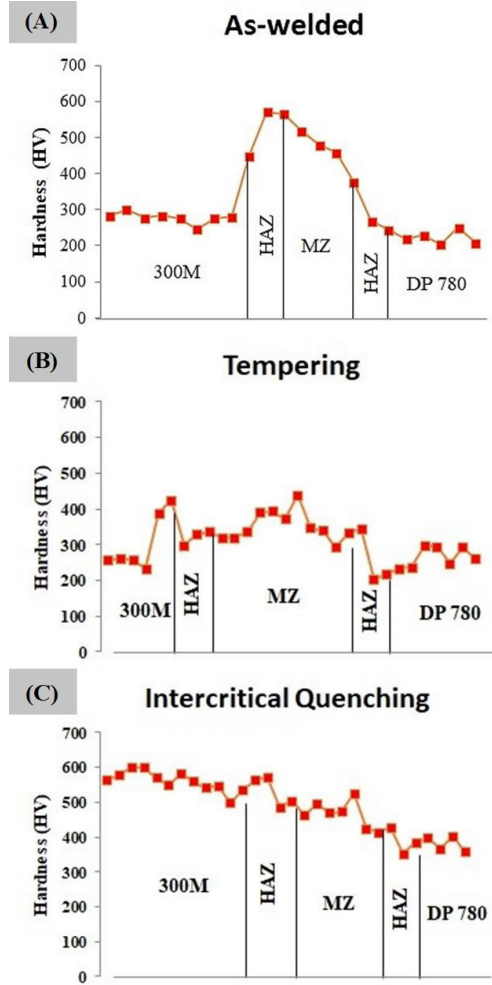


Figure 14. Microhardness profile of the specimens: (A) as-welded (B) tempering (c) intercritical quenching.

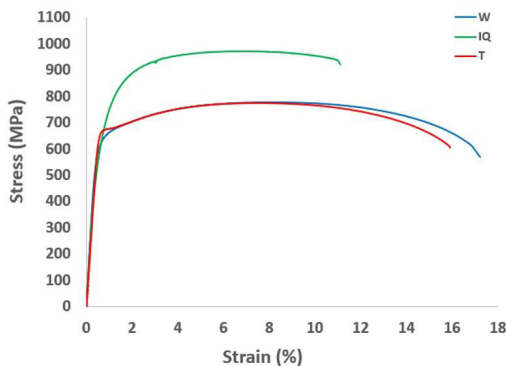


Figure 15. Representative engineering stress x strain curves for the 3 studied conditions, where W = As-welded, IQ = Intercritical Quenching and T = Tempering.

3.4. Fatigue tests

For a preliminary and exploratory evaluation of the fatigue resistance of the welds, 5 specimens of each condition were analyzed under uniaxial cycling loads, in a high cycle fatigue life regime ($10^4 < N < 10^6$). Important to notice, larger number of specimens would be required to properly determine SN curve for applications in mechanical projects²¹.

In Figure 16, represented stress amplitude x cycles curves for the 3 studied conditions, is possible to observe the as-welded specimens show the best results compared with other specimens.

The specimens submitted to the tempering treatment present the highest fatigue limit, at around 220 MPa, similar to the as-welded specimens. The specimens with intercritical quenching treatment present a lower fatigue performance, with a fatigue limit at around 120 MPa. This fact is intimately linked to the microstructural conditions: the significant increase of martensite volume fraction weakens the material, due to the reduction of ductility. The brittle microstructure reduces the plastic zone during maximum stress in the fatigue test. The velocity of crack propagation is higher, which leads to reduction in the fatigue life.

3.5. Fracture surface analysis

The crack started on the surface of the as-welded specimens, at one side of the specimens and grew, propagating inwards, at 90° to the direction of the tensile stresses applied during the fatigue test, in Figure 17A in Figure 17B, in addition to secondary microcracks in the propagation region represented in Figure 17C. In the final rupture region dimples are observed, indicating a ductile fracture mechanism, as shown in Figure 17D.

On the surface of the specimens with tempering treatment, the crack starts similarly to the specimens as-welded: at the side edge of the specimens, as shown in Figure 18A and Figure 18B. It is possible to observe the

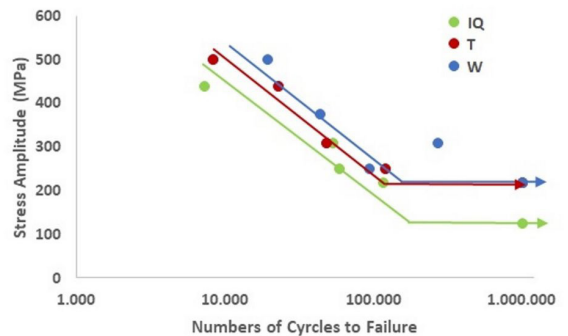


Figure 16. Stress amplitude x cycles curves for the 3 studied conditions, where W = As-welded, IQ = Intercritical Quenching and T = Tempering.

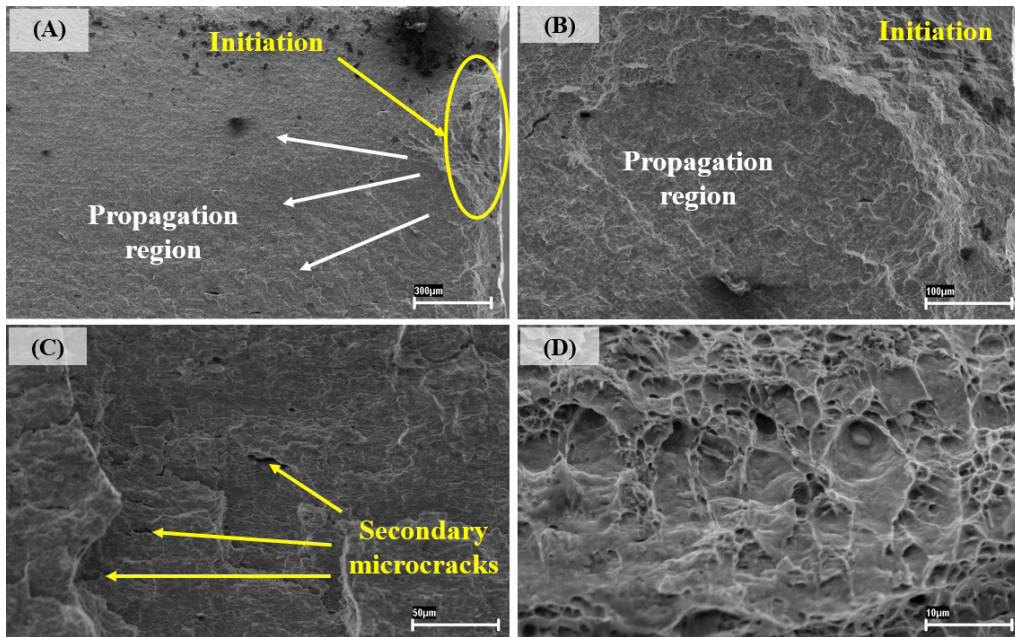


Figure 17. SEM (Secondary Electrons – SE). Surface of specimen as-welded (A) Overview: Initiation and propagation regions; (B) Initiation and propagation regions with higher magnification; (C) Secondary microcracks on propagation region and (D) final rupture region.

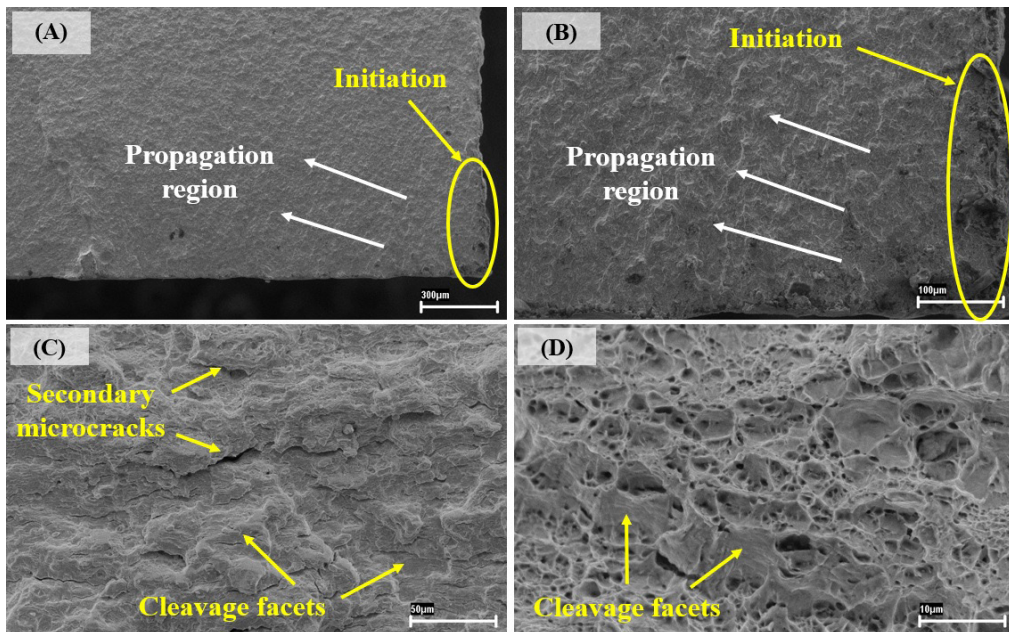


Figure 18. SEM (SE). Surface of specimen with tempering treatment (A) Overview: Initiation and propagation regions; (B) Initiation and propagation regions with higher magnification; (C) Secondary microcracks and cleavage facets on propagation region and (D) Final rupture region with dimples and some cleavage facets.

formation of secondary cracks in the propagation region as well as signs of plastic deformation during crack growth and cleavage facets, indicating the shear cut through the grains (transgranular fracture), as shown, respectively, in Figure 18C and Figure 18D. The blending of cleavage facets with dimple ruptures suggests a quasi-cleavage fracture

mechanism, which is often reported in embrittled steels, such as UHSS after quenching and tempering treatment²².

The crack initiation and propagation region of the specimens with intercritical quenching treatment is also located at the surface of the side edge of the specimens, as shown in Figure 19A and Figure 19B. In the propagation

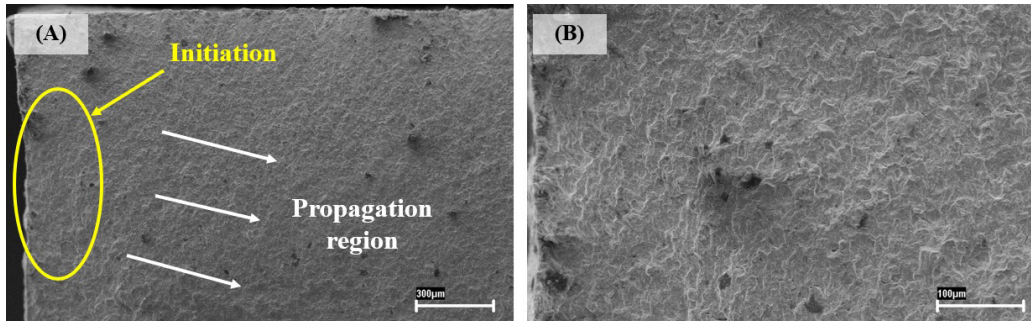


Figure 19. SEM (SE). Surface of specimen with intercritical quenching treatment. (A) Overview: Initiation and propagation regions and (B) Initiation and propagation regions with higher magnification.

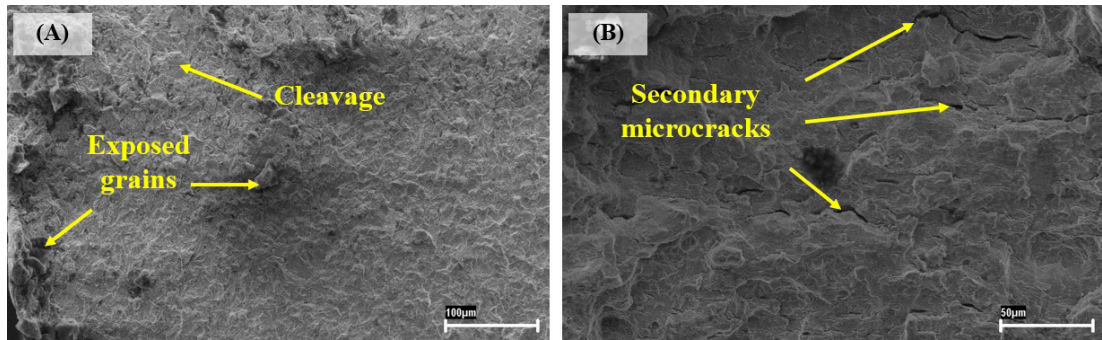


Figure 20. SEM (SE). Surface of specimen with intercritical quenching treatment. Propagation region: (A) indicating exposed grains, cleavage (quasi-cleavage and intergranular fracture mechanism) and (B) secondary microcracks.

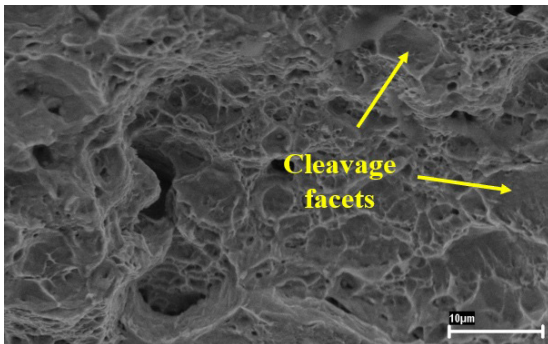


Figure 21. SEM (SE). Surface of specimen with intercritical quenching treatment. Final rupture region with dimples and some cleavage facets.

region, shown in Figure 20A and Figure 20B, in addition to the quasi-cleavage fracture mechanism, there are signs of grain boundaries exposure, indicating an intergranular fracture mechanism. This indicates a greater embrittlement and may explain the reduction in fatigue performance observed previously. In the final fatigue fracture region, shown in Figure 21, a quasi-cleavage fracture is observed again, indicated by the presence of dimple and cleavage facets.

4. Conclusions

In this work, samples of 300M and DP 780 steels were laser welded and submitted to 2 different heat treatment routes:

tempering and intercritical quenching. The results showed that the laser parameters used in the dissimilar laser welding process were efficient. After welding, there was a significant increase in hardness in the MZ and HAZ compared to the non-welded BM, however, without significant changes to the mechanical resistance and without compromising the ductility.

After the tempering heat treatment, the mechanical properties in tensile tests remained practically the same, with a slight reduction in elongation. In fatigue tests, the fatigue properties remained practically the same too, with a fatigue limit around 220 MPa. Was possible to observe the shear cut through the grains, indicating transgranular fracture, in addition, the blending of cleavage facets with dimple ruptures suggests a quasi-cleavage fracture mechanism.

For the intercritically quenched specimens, a significant increase in the ultimate tensile stress was observed, accompanied by a reduction in elongation both associated the increase the martensite, influence hardness and brittleness in the region and make a stress concentrator, which facilitating a nucleation and crack growth. These features impaired the fatigue performance, although an acceptable value was obtained: fatigue limit of 120 MPa, for a 10^6 cycles fatigue life. In addition the quasi-cleavage fracture mechanism observed, the exposure of grain boundaries indicate an intergranular fracture mechanism too.

5. References

1. ASM Handbook. Properties and selection: irons, steels, and high-performance alloys. 10th. ed. Ohio: Metals Handbook, 1990. 2521 p.

2. Lee WS, Su TT. Mechanical properties and microstructural features of AISI 4340 high-strength alloy steel under quenched and tempered conditions. *J Mater Process Technol.* 1997;87:198-206.
3. Anazawa RM, Abdalla AJ, Hashimoto TM, Pereira MS, Carrer GR, Elisei CCA et al. Aumento do limite de escoamento de um aço multifásico devido ao envelhecimento por deformação e efeito TRIP. *Rev Bras Apl Vácuo.* 2008;27(1):19-23.
4. Sakai PR, Silva DF, Lima MSF, Siqueira RHM, Abdalla AJ. Mechanical and microstructural characterization of plasma welded joints of 18 Ni-300 maraging steels subjected to repairs. *J Aircr Spacecr Technol.* 2021;5(1):5-20.
5. Carvalho SM, Lima MSF. Laser beam welding tempered 300M ultrahigh mechanical strength steel. *J Braz Soc Mech Sci Eng.* 2012;34:18-23.
6. Cardoso ASM, Abdalla AJ, Baptista CARP, Lima MSF. Comparison of high cycle fatigue in 4340 and 300M steel welded with fiber laser. *Adv Mat Res.* 2014;891-892:1507-12.
7. Santos D, Vasconcelos G, Abdalla AJ, Lima MSF, Souza F No. Surface characterization in a 300 M bainitic steel laser carburizing. *Procedia Eng.* 2015;114:322-9.
8. Correard GC. Caracterização da microestrutura e das propriedades mecânicas de aços avançados de alta resistência soldados a laser [thesis]. São José dos Campos: Instituto Tecnológico de Aeronáutica; 2018.
9. Daneshpour S, Riekehr S, Koçak M, Gerritsen CHJ. Mechanical and fatigue behaviour of laser and resistance spot welds in advanced high strength steels. *Sci Technol Weld Join.* 2009;14(1):20-5.
10. Xu HF, Zhao J, Cao WQ, Shi J, Wang CY, Wang C et al. Heat treatment effects on the microstructure and mechanical properties of a medium manganese steel (0.2C-5Mn). *Mater Sci Eng A.* 2012;532:435-42.
11. CGEE: Centro de Gestão e Estudos Estratégicos. *Materiais avançados no Brasil 2010-2022.* Brasília, DF: CGEE; 2010.
12. Ahiale GK, Oh Y. Microstructure and fatigue performance of butt-welded joints in advanced high-strength steels. *Mater Sci Eng A.* 2014;597:342-8.
13. Park G, Kim B, Kang Y, Kang H, Lee C. Characterization of bond line discontinuities in a high-Mn TWIP steel pipe welded by HF-ERW. *Mater Charact.* 2016;118:14-21.
14. Wang M, Tasan CC, Ponge D, Dippel AC, Raabe D. Nanolaminate transformation-induced plasticity–twinning-induced plasticity steel with dynamic strain partitioning and enhanced damage resistance. *Acta Mater.* 2015;85:216-28.
15. Sarkar S, Militzer M, Poole W, Fazeli F. Microstructural evolution in a complex-phase steel. In: *Materials Science and Technology Conference and Exhibition; 2007; Detroit. Proceedings.* Detroit: Greyden Press; 2007. p. 61-72.
16. Krajewski S, Nowacki J. Dual-phase steels microstructure and properties consideration based on artificial intelligence techniques. *Arch Civ Mech Eng.* 2014;14(2):278-86.
17. Ashrafi H, Shamanian M, Emadi R, Saeidi N. A novel and simple technique for development of dual phase steels with excellent ductility. *Mater Sci Eng A.* 2017;680:197-202.
18. Shome M, Tumuluru M, editors. *Welding and joining of Advanced High Strength Steels (AHSS).* Cambridge: Elsevier; 2015.
19. American Society for Testing and Materials. E466: standard practice for conducting force controlled constant amplitude axial fatigue tests of metallic materials. West Conshohocken, PA: ASTM International; 2021.
20. American Society for Testing and Materials. E8/E8M: standard test methods for tension testing of metallic materials. West Conshohocken, PA: ASTM International; 2021.
21. American Society for Testing and Materials. E739-10: standard practice for statistical analysis of linear or linearized stress-life (S-N) and strain-life (ϵ -N) fatigue data. West Conshohocken, PA: ASTM International; 2015.
22. Watanabe T. Grain boundary sliding and stress concentration during creep. *Metall Trans, A, Phys Metall Mater Sci.* 1983;14A(4):531-45.